AIAA JOURNAL
Vol. 39, No. 9, September 2001

Time-Domain Impedance Boundary Conditions with Mean Flow Effects

Hongbin Ju* and K.-Y. Fung†
Hong Kong Polytechnic University, Kowloon, Hong Kong, People's Republic of China

The development of time-domain impedance boundary condition (TDIBC) for prediction of aeroacoustics in wall bounded flows is explored. The presence of a flow and its boundary layer over a wave-absorbing surface complicates the modeling and implementation of TDIBC. Considered here are three different approaches to account for the effects of wave refraction, absorption, reflection, and convection at a wave-absorbing wall. They are the effective plane-wave impedance in a slip flow, convection-modified impedance in a slip flow, and wave reflection in a mean shear-layer flow. Their validity, effectiveness, stability, and implementation in time-domain finite-difference schemes will be discussed. The schemes and methods developed here are benchmarked and compared with experiment and other methods.

Introduction

THE convective environment of a wall-bounded mean flow complicates the propagation, reflection, and refraction of acoustic disturbances. Experiments and analyses have shown that at high Mach numbers the boundary layer has a strong shielding effect against absorption of waves by surface treatment.[1–3] In a duct the attenuation could be so modified by a mean flow to cause an increase in sound pressure on the downstream walls and a reduction on the upstream walls.[4] High-pressure-gradient induced internal flow in the material could change its absorptive properties. The experiment and analysis of Ref. 5 demonstrated increases of material resistance and reactance with flow rate. The directional wave evolution processes and the generation of oblique or transverse waves in ducts caused by shear-layer refraction were recognized after the recent time-domain analysis of Ref. 6 and the direct Navier–Stokes simulations of Ref. 4. The classical approaches for prediction and analysis of such flow disturbances have largely been based on normal mode expansions in frequency domain.[7] However, the assumption of normal modes in classical analyses was shown to be inadequate for the analyses of some shear flow experiments.[8] The availability of a general method will allow a better understanding of these flow disturbances and lead to more effective means for their control.

The effects of an absorptive wall on the waves in a wall-bounded flow have been treated either as disturbances satisfying the impedance condition $\hat{p} = Z\hat{v}$ in the mean shear-layer flow with impedance $Z(\omega, \theta)$ or in the mean freestream of Mach number M_0 with the effective plane-wave impedance $Z' = Z(1 + M_0 \sin\theta)$.[7,9] Here $\hat{p}$ and $\hat{v}$ are respectively the perturbed pressure and its induced velocity component toward the wall decomposed as plane harmonic waves of frequency ω and incident angle θ to the wall normal direction. The resolution of the thin boundary layer requires in general more computational resources than that of the mean freestream, but the specification of the effective incident angle is not straightforward for nonplanar waves. The use of a convection-modified impedance condition

$$\hat{v} = \frac{\hat{p}}{Z} + M_0(i\omega Z)^{-1}\frac{\partial \hat{p}}{\partial x}$$

to account for the wave angle by differentiation in the x direction tangent to wall has been proposed.[10] Both approaches have been studied in detail in frequency domain.[7] All variables unless specified are dimensionless with $\hat{p}$ normalized by the dynamic sound pressure $\rho_0 C_0^2$ of free air of density ρ_0; induced velocity $\hat{v}$ by C_0; x by the characteristic length L; and ω by C_0/L unit traveled by sound of speed C_0; Z by $\rho_0 C_0$; and the caret denotes Fourier components with time dependence $e^{i\omega t}$.

In time domain a straightforward application of operational mathematics to convert an expansion of $Z(\omega)$ in powers of $(i\omega)^k$ to corresponding operators in $(\mathrm{d}^k/\mathrm{d}t^k)$ would in general lead to unstable boundary conditions.[11] Tam and Auriault[12] addressed the instability problem and demonstrated the construction of stable impedance-dependent schemes for reflection of harmonic waves and banded pulses in one dimension. Their analysis on the convection-modified impedance condition suggested an instability of Kelvin–Helmholtz type and proposed the use of impedance $Z'(M_0, \omega)$ measured under flow condition to avoid this instability. Özyörük et al.[13,14] implemented the convection-modified impedance in the form of a z transform and found conditionally stable numerical solutions. Fung et al.[11] proposed a method for derivation of stable time-domain impedance boundary condition (TDIBC) from the reflection coefficient $\hat{W} = (1 - Z)/(1 + Z)$ and benchmarked their method with analytic solutions, including the reflection of a Gaussian-like pulse in two dimensions.

We will explore here the construction of TDIBC using 1) the effective plane-wave impedance, 2) the convection-modified impedance, and 3) mean shear-layer flow bounded by an impedance surface. Effects caused by convection, shear-layer refraction, and impedance discontinuity will be studied. Numerical results using these approaches will be compared with analytical solutions and available experimental data to support their efficacy.

Time-Domain Impedance Model

The time-domain reflection process, which relates the incident wave v^+ to the reflected wave v^- at a wall, is as follows [Eq. (9), Ref. 11]:

$$v^-(t) = \int_{-\infty}^{\infty} W(\tau)v^+(t-\tau)\,\mathrm{d}\tau \tag{1}$$

where $W(\tau)$ is the Fourier inverse transform of the reflection coefficient $\hat{W}(\omega) \equiv (1 - Z)/(1 + Z)$, and when expressed in an algebraic function of ω can assume the form

$$W(\tau) = \begin{cases} i\displaystyle\sum_{\mathrm{Im}(\Omega_j)>0} \mathrm{residue}\,[\hat{W}(\omega), \Omega_j]e^{i\Omega_j\tau}, & \tau \geq 0 \\ -i\displaystyle\sum_{\mathrm{Im}(\Omega_j)<0} \mathrm{residue}\,[\hat{W}(\omega), \Omega_j]e^{i\Omega_j\tau}, & \tau < 0 \end{cases} \tag{2}$$

where Ω_j is the jth root of $1 + Z(\omega) = 0$. The reflection function $W(\tau)$ is impulselike $e^{i\Omega_j\tau}$ when none of the roots is purely real, and

Received 25 July 2000; revision received 24 February 2001; accepted for publication 2 March 2001.

*Postdoctoral Research Fellow, Mechanical Engineering Department. Member AIAA.

†Professor, Mechanical Engineering Department; mmkyfung@polyu.edu.hk. Associate Fellow AIAA.

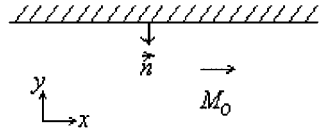

Fig. 1 Flow parallel to impedance wall.

the requirement that the total reflection be a real quantity implies that only purely real or pairs of $\{\text{residue}[\hat{W}(\omega), \Omega_j]e^{i\Omega_j\tau}\}$ are acceptable choices.

The integral form equation (1) poses two problems: finding roots Ω_j and ensuring the positiveness of their imaginary parts. For example, the three-parameter impedance model

$$Z = R_0 + i(-X_{-1}/\omega + X_1\omega) \tag{3}$$

with roots $\Omega_{1,2} = [(1+R_0)/2X_1]i \pm \sqrt{\{(X_{-1}/X_1) - [(1+R_0)/2X_1]^2\}}$ represents a damped harmonic oscillator of acoustic mass X_1, stiffness X_{-1}, and resistance R_0. The corresponding time-equivalent reflection impulse has the form

$$W(t) = \tilde{W}(t)H(t) - \delta(t)$$

$$\tilde{W}(t) = (2/X_1)[\cos(\beta t) - (\alpha/\beta)\sin(\beta t)]e^{-\alpha t} \tag{4}$$

where $H(t)$ is the Heaviside function, $\alpha = (1+R_0)/2X_1$ the damping rate, $\beta = \sqrt{(\omega_0^2 - \alpha^2)}$ the oscillation frequency, and $\omega_0 = \sqrt{(X_{-1}/X_1)}$ the natural frequency of the harmonic oscillator. This three-parameter model can be used to represent narrowband impedance variations by choices of X_1, X_{-1}, and R_0. For broadband problems the impedance data can be constructed by a set of such damped harmonic oscillators.[15]

TDIBC with Convective Effects

For the coordinate system shown in Fig. 1, the nondimensional boundary condition on the acoustic velocity at the upper wall can be stated as[10]

$$\hat{v} = \hat{p}/Z + (1/i\omega)\boldsymbol{M}_0 \cdot \nabla(\hat{p}/Z) - (\hat{p}/i\omega Z)\boldsymbol{n} \cdot (\boldsymbol{n} \cdot \nabla \boldsymbol{M}_0) \tag{5}$$

where $\boldsymbol{n}$ is the unit normal vector of the wall directed into the fluid (Fig. 1) and $\boldsymbol{M}_0$ the mean Mach-number vector. For a plain impedance wall in two dimensions, the last term of Eq. (5) can be dropped to give the convection-modified impedance condition

$$\hat{v} = \frac{\hat{p}}{Z} + M_0(i\omega Z)^{-1}\frac{\partial \hat{p}}{\partial x} \tag{6}$$

Assuming plane waves of the form $\exp[i(\omega t - k_x x)]$, Eq. (6) can further be reduced to

$$\hat{v} = \hat{p}/Z' \tag{7}$$

where $Z' = Z(1 + M_0 \sin\theta)$ can be seen as the effective plane-wave impedance with the effective incident wave angle $\theta = \sin^{-1}[k_x/(\omega - k_x M_0)]$.

With the modified reflection coefficient as $\hat{W}' \equiv (1-Z')/(1+Z')$, Eq. (7) corresponds to a modified harmonic oscillator of resistance $R_0' = R_0(1 + M_0\sin\theta)$, stiffness constant $X_{-1}' = X_{-1}(1 + M_0\sin\theta)$, and mass $X_1' = X_1(1 + M_0\sin\theta)$. It has the same natural frequency as that of the primary impedance $\omega_0' = \omega_0$, but the mean flow decreases the damping coefficient and increases the oscillating frequency as a wave moves toward downstream, i.e., $\alpha' = [(1 + M_0\sin\theta)^{-1} + R_0]/2X_1$, $\beta' = \sqrt{(\omega_0^2 - \alpha'^2)}$, and vice versa. The corresponding effective reflection impulse for TDIBC is

$$W'(t) = [2/(1 + M_0\sin\theta)X_1][\cos(\beta' t) - (\alpha'/\beta')\sin(\beta' t)]e^{-\alpha' t}H(t) - \delta(t) \tag{8}$$

which can be implemented efficiently by a recursive formula.[15]

For implementation of Eq. (6) as TDIBC, Fung et al.[11] proposed the formula

$$\left[1 + M_0\hat{W}_{II}(\omega)\frac{\partial}{\partial x}\right]\hat{v}^- = \left[\hat{W}(\omega) + M_0\hat{W}_{II}(\omega)\frac{\partial}{\partial x}\right]\hat{v}^+ \tag{9}$$

where $\hat{v}^\pm = \hat{v} \pm \hat{p}$ and $\hat{W}_{II}(\omega) = 1/[i\omega(1+Z)]$. They also gave the corresponding convolution process

$$v^-(t) + M_0\int_{-\infty}^{+\infty} W_{II}(t-\tau)\frac{\partial}{\partial x}v^-(\tau)\,d\tau = \int_{-\infty}^{+\infty}\left[W(t-\tau) + M_0 W_{II}(t-\tau)\frac{\partial}{\partial x}\right]v^+(\tau)\,d\tau \tag{10}$$

If the impedance model Eq. (3) is used, $W(t)$ takes the form of Eq. (4) and $W_{II}(t)$ has the form

$$W_{II}(t) = (X_1\beta)^{-1}\sin(\beta t)e^{-\alpha t}H(t)$$

and the convection-modified TDIBC can be numerically implemented as

$$v^-(t) = \Delta t\sum_{j=0}^{N} q_j\tilde{W}(j\Delta t)v^+(t - j\Delta t) - v^+(t) + 2M_0\Delta t\sum_{j=1}^{N} q_j W_{II}(j\Delta t)\frac{\partial}{\partial x}p(t - j\Delta t)$$

where q_j are quadrature coefficients, Δt is the time increment, N a sufficiently large number to represent the integrals in Eq. (10), and the convective derivative of $v^-(t)$ has been removed because of $W_{II}(0) = 0$. If the trapezoidal time integration is used, the preceding equation reduces to

$$v^-(t) = \Delta t S_I(t) + 2M_0\Delta t S_{II}(t) - (\Delta t/X_1 + 1)v^+(t) \tag{11}$$

where

$$S_I(t) = \sum_{j=0}^{N}\tilde{W}(j\Delta t)v^+(t - j\Delta t)$$

$$S_{II}(t) = \sum_{j=0}^{N} W_{II}(j\Delta t)\frac{\partial}{\partial x}p(t - j\Delta t)$$

or in the recursive form

$$S_I(t) = 2\cos(\beta\Delta t)e^{-\alpha\Delta t}S_I(t-\Delta t) - e^{-2\alpha\Delta t}S_I(t-2\Delta t) + (2/X_1) \times \{v^+(t) - [\cos(\beta\Delta t) + \alpha\sin(\beta\Delta t)/\beta]e^{-\alpha\Delta t}v^+(t-\Delta t)\}$$

$$S_{II}(t) = 2\cos(\beta\Delta t)e^{-\alpha\Delta t}S_{II}(t-\Delta t) - e^{-2\alpha\Delta t}S_{II}(t-2\Delta t) + \frac{1}{X_1\beta}\sin(\beta\Delta t)e^{-\alpha\Delta t}\frac{\partial}{\partial x}p(t-\Delta t)$$

for which the choice of N is immaterial and the equivalent integral is extended indefinitely.

Numerical Scheme for Acoustics in Shear Flow

Refraction effects of a boundary layer over an impedance wall in a high-speed flow have been treated analytically by Goldstein and Rice using equivalent impedance values via parabolic cylinder functions.[16] Özyörük et al.[13] considered the mass deficit of a fully developed laminar duct flow and proposed the use of the average speed $M_{\text{ave}} = 2/3M_0$ to account for refraction effects, and later Özyörük and Long[14] solved the wave equations with a shear flow profile. Here, we extend the approach of Fung et al.[11,17] to include a nonuniform mean flow.

The two-dimensional linear Euler equations with nonuniform mean flow can be expressed as

$$\frac{\partial U}{\partial t} + A_x\frac{\partial U}{\partial x} + A_y\frac{\partial U}{\partial y} + (B_x + B_y)U = S \tag{12}$$

where

$$U = \begin{bmatrix} u \\ v \\ p \end{bmatrix}, \qquad A_x = \begin{bmatrix} U_0 & 0 & C_0^2 \\ 0 & U_0 & 0 \\ 1 & 0 & U_0 \end{bmatrix}$$

$$A_y = \begin{bmatrix} V_0 & 0 & 0 \\ 0 & V_0 & C_0^2 \\ 0 & 1 & V_0 \end{bmatrix}, \qquad B_x = \frac{\partial}{\partial x}\begin{bmatrix} U_0 & 0 & C_0^2 \\ V_0 & 0 & 0 \\ \ell_n \rho_0 & 0 & 0 \end{bmatrix}$$

$$B_y = \frac{\partial}{\partial y}\begin{bmatrix} 0 & U_0 & 0 \\ 0 & V_0 & C_0^2 \\ 0 & \ell_n \rho_0 & 0 \end{bmatrix}, \qquad S = \begin{bmatrix} f_x \\ f_y \\ f_\rho \end{bmatrix}$$

U_0, V_0 are, respectively, the mean velocities in the x and y directions; ρ_0 mean density; and C_0 local sound speed, which can differ for a shear flow from the reference sound speed C (340 m/s). All other lowercase variables in the preceding equation denote perturbation quantities. As stated before, distance, speed, and time have been nondimensionalized respectively by characteristic length L (grid length), sound speed C and L/C, pressure by local dynamic pressure $\rho_0 C_0^2$, fluctuating volume f_ρ by local density ρ_0, and fluctuating force $\boldsymbol{f} = (f_x, f_y)$ by $\rho_0 C^2/L$ for simplicity.

Equation (12) can be split into dimensional equation sets with refraction terms averaged as

$$\frac{\partial U}{\partial t} + A_x \frac{\partial U}{\partial x} + \frac{1}{2}(B_x + B_y)U = \frac{1}{2}S$$

$$\frac{\partial U}{\partial t} + A_y \frac{\partial U}{\partial y} + \frac{1}{2}(B_x + B_y)U = \frac{1}{2}S \tag{13}$$

or in characteristic forms for a parallel flow in the x direction with shear distribution $M_x(y)$ as

$$\frac{\partial}{\partial t}\begin{bmatrix} v \\ u^+ \\ u^- \end{bmatrix} + \begin{bmatrix} M_x & 0 & 0 \\ 0 & M_x + 1 & 0 \\ 0 & 0 & M_x - 1 \end{bmatrix} \frac{\partial}{\partial x}\begin{bmatrix} v \\ u^+ \\ u^- \end{bmatrix}$$

$$+ \frac{1}{2}\begin{bmatrix} 0 \\ v\dfrac{\partial M_x}{\partial y} \\ v\dfrac{\partial M_x}{\partial y} \end{bmatrix} = \frac{1}{2}\begin{bmatrix} f_y \\ f_x + f_\rho \\ f_x - f_\rho \end{bmatrix}$$

$$\frac{\partial}{\partial t}\begin{bmatrix} u \\ v^+ \\ v^- \end{bmatrix} + \begin{bmatrix} 0 & 0 & 0 \\ 0 & 1 & 0 \\ 0 & 0 & -1 \end{bmatrix} \frac{\partial}{\partial y}\begin{bmatrix} u \\ v^+ \\ v^- \end{bmatrix}$$

$$+ \frac{1}{2}\begin{bmatrix} v\dfrac{\partial M_x}{\partial y} \\ 0 \\ 0 \end{bmatrix} = \frac{1}{2}\begin{bmatrix} f_x \\ f_y + f_\rho \\ f_y - f_\rho \end{bmatrix}$$

where $u^\pm = u \pm p$, $v^\pm = v \pm p$. These are six uncoupled simple wave equations. The principal waves are advanced for each time increment Δt using the compact scheme C3N (with fourth-order spatial and second-order temporal accuracy) of Fung et al.[17] The refraction and source terms are handled explicitly to second order. The characteristic determination of exit wave at end points, Eq. (3) in Ref. 17, is revised to include refraction and source terms.

At the inlet of the source plane, the transparent acoustic source gives directly the far upstream characteristic variable $u^+ = 2p_A \sin(\omega t)$ for plane waves. Exact distributions of pressure amplitude p_A and frequency ω are unavailable from the shear flow experiments. Uniform distributions are assumed. The convective characteristic variable v at the inlet and the receding acoustic characteristic variable u^- at the outlet boundaries in x direction can assume radiation boundary conditions such as Giles,[18] but for the flow-impedance tube studied next, these two variables can simply be set to zero. In the impedance wall bounded y direction, TDIBC of Eqs. (8) and (11) are implemented, including solid walls as $W(t) = -1$.

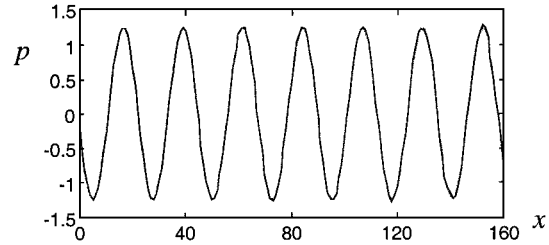

Fig. 2 Pressure distributions at $t = 200$ along the impedance wall caused by the reflection of a $\theta = 45$-deg incident plane wave with $\omega = 0.5313$ and $Z = 1 + i$ in slip flow of $M_0 = 0.5$: ——, Eq. (8); - - - -, Eq. (11); and ·····, analytical solution of Ref. 19.

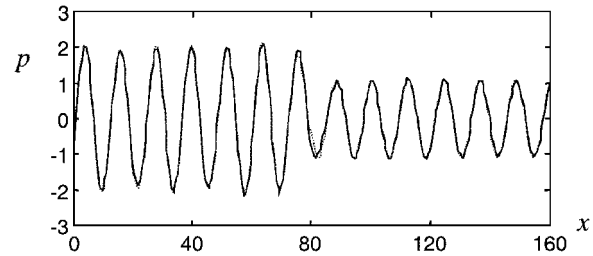

Fig. 3 Pressure distributions at $t = 300$ along the mixed wall caused by the reflection of a $\theta = 45$-deg incident plane wave with $\omega = 0.7388$, $Z = 1 + i$, and $M_0 = 0$: ——, numerical and ·····, analytical solution Eq. (A2).

Validation of Methods

We first validate the effective plane-wave TDIBC (8) and convection-modified TDIBC (11), using an exact solution for plane waves.[19] The computation domain is $x \in [0, 160] \cup y \in [0, 30]$ with unit length $L = 5$ mm and impedance wall at $y = 0$. Analytical acoustic disturbances with exciting frequency $\omega = 0.5313$ are given at the inlet boundaries $x = 0$ and $y = 30$, and Giles' radiation condition[18] is used at $x = 160$. A minimum grid resolution of 10 points per wavelength is sufficient for all computations. Figure 2 shows the excellent agreement between the analytical and numerical results.

In practical cases and the case considered next the wall acoustic properties are often not uniform but lined with mixed impedance patches. Before the method is compared with the experiment where the in situ impedance value at a discontinuity may be ambiguous, an analytical solution of plane wave reflection at an impedance discontinuity without flow was derived (Appendix) from De Jong's model. Figure 3 compares the numerical and analytical pressures with the same wall geometric as in the preceding case, but the hard wall changed abruptly into a soft wall at $x = 80$. The agreement everywhere else is excellent except the small phase discrepancy at the impedance discontinuity where the validity of the analytical solution is questionable.

Sound Fields in Flow-Impedance Tube

An experiment on the acoustics of a flow-impedance tube was conducted in the Flow-Impedance Test Laboratory of NASA Langley Research Center.[20] A schematic of the test section is shown in Fig. 4. The first cutoff frequency based on the tube height without flow is 3.287 kHz. The sound fields over the range of exciting frequency f_e from 0.5 to 3 kHz are expected to be mainly one-dimensional, and incident waves at 90 deg grazing the impedance wall are assumed. Here f_e in kilohertz is dimensional and related to the circular frequency ω by $f_e = \omega C/(2000\pi L)$. The measured specific impedance values are listed in Table 1. For simple TDIBC

Table 1 Specific impedance data of a constant depth ceramic tubular liner[20]

f_e, kHz	Z
0.5	0.41–1.56i
1.0	0.46+0.03i
1.5	1.08+1.38i
2.0	4.99+0.25i
2.5	1.26−1.53i
3.0	0.69−0.24i

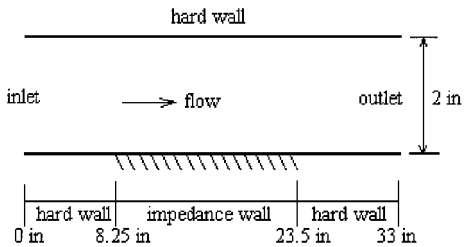

Fig. 4 Schematic of the flow-impedance tube.

implementation single impedance model of Eq. (3) with a different set of acoustic mass X_1, stiffness X_{-1}, and resistance R_0 chosen to match only the correct value of Z in Table 1 for each frequency is used. Plotted in Figs. 5a–5e are computed and measured acoustic pressure distributions along the upper solid wall at different frequencies for $M_0 = 0$. Similar results are shown in Figs. 6–8, respectively, for slip flows of $M_0 = 0.1$, 0.3, and 0.5. Ten points per wavelength (PPW) for the shortest wave are sufficient to resolve the wave decay. Both TDIBC (8) and TDIBC (11) give effectively same results, but the use of Eq. (11) is only conditionally stable. Corresponding results, if available, from Özyörük et al.,[13,14] for which a grid resolution better than 22.7 PPW is needed compared to not more than 10 PPW for the present method, are also shown for comparison.

Stability at Impedance Discontinuity

The implementation of TDIBC (8) is straightforward and unconditionally stable,[11] but the implementation of TDIBC (11) can lead to numerical instability. For plane waves of the form $\exp[i(\omega t - k_x x)]$ along the wall in x, Eq. (9) implies the reflection amplification factor

$$A_a \equiv \frac{\hat{v}^-}{\hat{v}^+} = \frac{(1-Z)/(1+Z) - ik_x M_0 \hat{W}_{II}(\omega)}{1 - ik_x M_0 \hat{W}_{II}(\omega)} \tag{14}$$

which is bounded by 1, i.e., $|A_a| \leq 1$, if the physical constraint on the wave number

$$k_x \leq \omega / M_0 \tag{15}$$

is satisfied. This implies that Eq. (10) or (11) is stable for receding waves of $k_x < 0$ and for advancing waves in a subsonic flow of $0 < k_x = \omega/(1 + M_0 \sin\theta)$. The forms of Eqs. (9) and (14) suggest the strong dependence of A_a on parameter $T_c = |k_x M_0 \hat{W}_{II}(\omega)|$, a product of the wave number k_x of the physical and spurious waves present in a solution field, flow speed M_0, and wall impedance model. In the limit of T_c or $M_0 \to 0$, A_a reduces to the reflection coefficient $\hat{W}$, which is bounded by one. Equation (15) suggests that instability occurs at low frequencies and high Mach numbers, which is consistent with the computations using TDIBC (11) summarized in Table 2. The instability when occurred started at impedance discontinuities or inlet corners as exemplified in Fig. 9. Figure 10 shows typical variations of $|A_a|$ with frequency for plane waves (solid line) and for fixed wave numbers (long and short dashed lines). At impedance discontinuities or frontal point of an impedance wall, a finite difference scheme can sustain spurious waves of high complex wave numbers for which $|A_a| > 1$. For given flow speed and impedance the variation of the wave number k_x of the most amplified wave with frequency f_a can be defined as the locus of amplification peaks, the triangles in Fig. 10, confirming the amplification of spurious waves at low frequencies. Table 2 reveals the existence of a stability threshold value of $T_c(f_a) = |k_x(f_a) M_0 \hat{W}_{II}(f_a)| < 0.85$

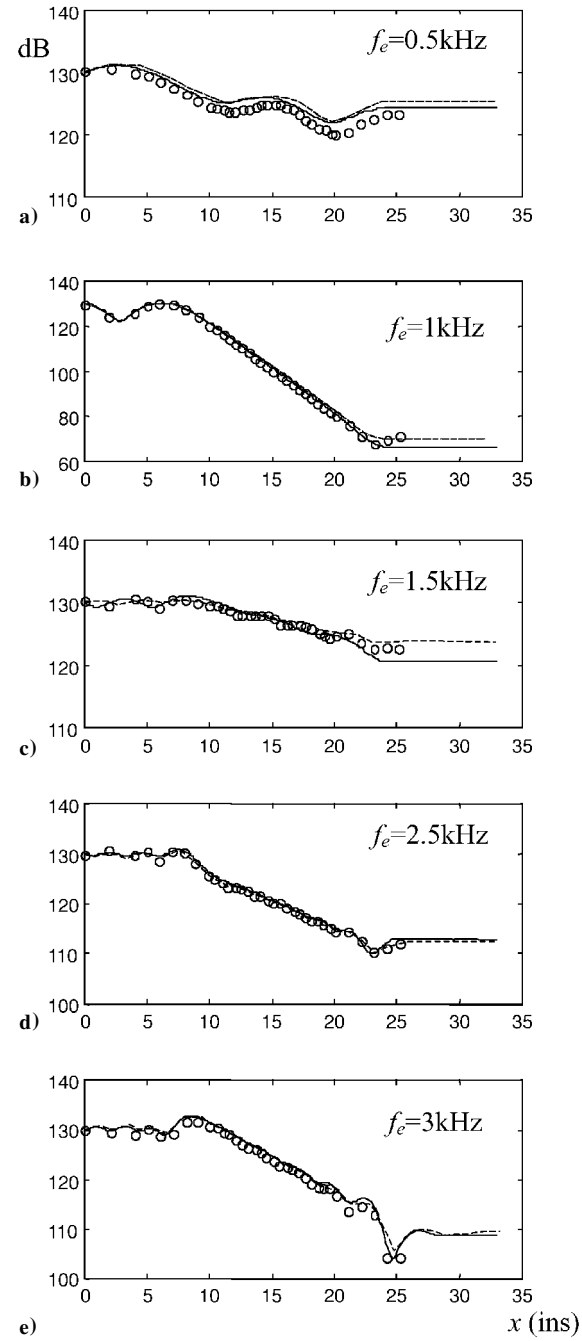

Fig. 5 Sound pressure along the upper wall at different frequencies for $M_0 = 0$: ——, present calculation with TDIBC (11); ∘∘∘, experiment; and - - - -, Ref. 13.

when evaluated at the most amplifying frequency f_a instead of the forcing frequency f_e. Because the range of k_x for numerically supported waves decreases with increasing grid spacing Δx, a coarser grid (256×17) indeed gave a stable solution when solution on the finer grid (529×33) was marginally unstable for $M_0 = 0.5$ and $f_e = 3$ kHz. Similarly, if operator smoothing, weighted averaging of neighboring differenced values of $\partial p(t - \Delta t)/\partial x$ in TDIBC (11) at the impedance transition region, is applied as a simple low-pass digital filter of spurious waves, instability can also be suppressed, resulting in the stable solution shown in Fig. 11. Another effective way to suppress instability for narrowband applications is to reduce the magnitude of $|\hat{W}_{II}(f_a)|$ by choosing a large X_1 for the impedance model of Eq. (3). The use of $Z = 0.69 + i(-0.3263/\omega + 9.167\omega)$ instead of $Z = 0.69 + i(-0.1868/\omega + 4.667\omega)$ gives a smaller value of $T_c(f_a) = 0.8181$ at $f_a = 3.0678$ kHz, the same value of Z at $f_e = 3$ kHz, and a stable solution for $M_0 = 0.5$. For broadband applications the use of an appropriate low-pass digital filter should

Table 2 Stability of TDIBC (11)

	$M_0 = 0.1$			$M_0 = 0.3$			$M_0 = 0.5$		
f_e, kHz	f_a, kHz	$T_c(f_a)$	Eq. (11)	f_a, kHz	$T_c(f_a)$	Eq. (11)	f_a, kHz	$T_c(f_a)$	Eq. (11)
0.5	0.6647	0.7396	Stable	1.5339	1.1601	Unstable	1.8748	1.4906	Unstable
1.0	0.6476	0.8238	Stable	1.2783	1.3194	Unstable	1.6191	1.5833	Unstable
1.5	0.5113	0.7096	Stable	1.0226	1.1726	Unstable	1.2442	1.5063	Unstable
2.0	0.3409	0.1412	Stable	1.0226	0.3442	Stable	1.1930	0.5325	Stable
2.5	0.3750	0.1540	Stable	1.5339	0.4275	Stable	2.7269	0.6010	Stable
3.0	0.3750	0.2656	Stable	1.7043	0.6832	Stable	2.8974	0.8563	Unstable

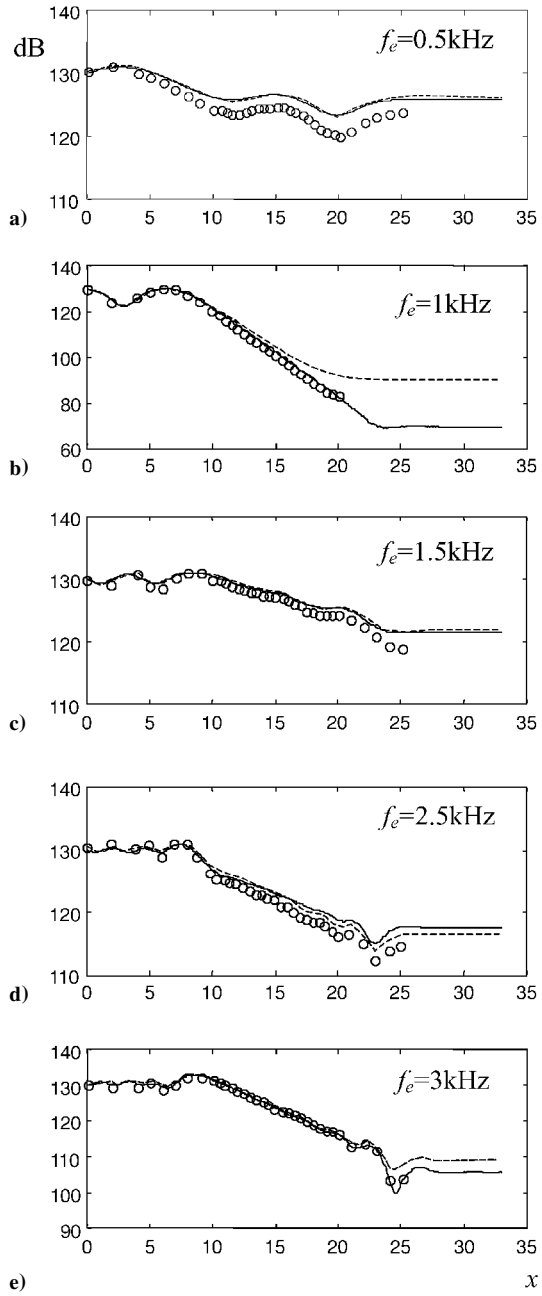

Fig. 6 Sound pressure along the upper wall at different frequencies in slip flow $M_0 = 0.1$: ——, present calculation with TDIBC (11); ∘∘∘, experiment; and - - - -, Ref. 13.

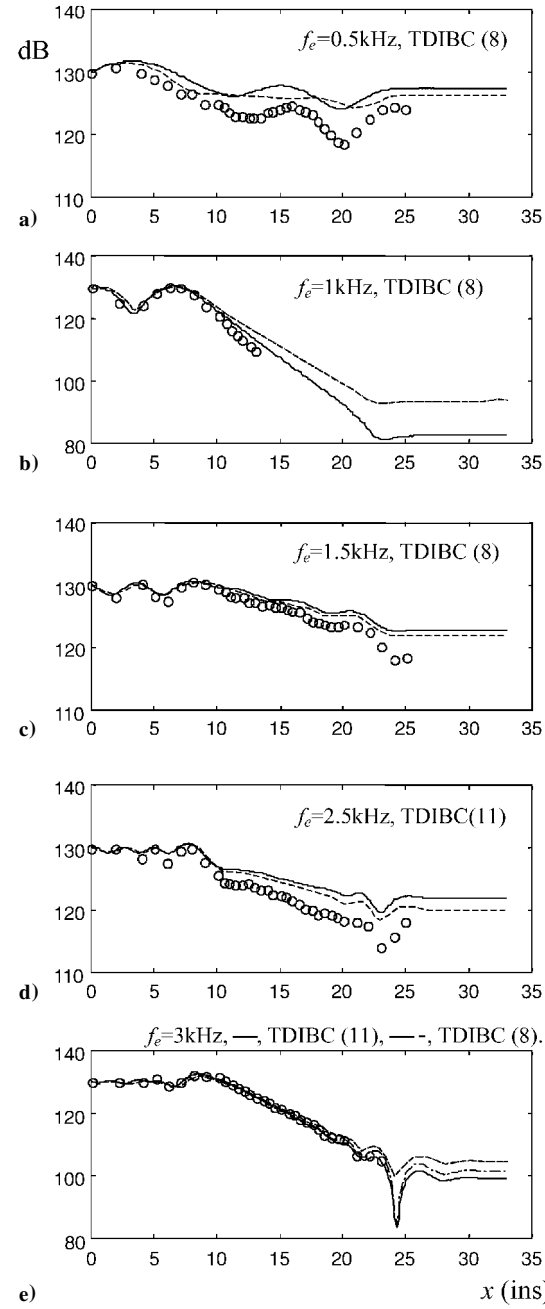

Fig. 7 Sound pressure along the upper wall at different frequencies in slip flow $M_0 = 0.3$: ——, present; ∘∘∘, experiment; and - - - -, Ref. 13.

effectively enforce Eq. (15) to ensure stability so long as the filter does not alter significantly the physical dispersion relation.

Comparison with Experiments

Table 3 summarizes the agreement between the measured and computed results. It shows that for highly absorptive impedance, at $f_e = 3$ kHz, the agreement is good for all flow speeds. But for highly reflective impedance, at $f_e = 0.5$ kHz, the computed results consistently overestimate the pressure level (Figs. 6a, 7a, and 8a). The use of an effective mean velocity, e.g., $M_{\text{ave}} = 2/3M_0$, can give some improvement (Figs. 8b and 8d). The setting of the effective incident angle at grazing $\theta = 90$ deg is satisfactory for all cases here, and little improvement can be expected by varying the effective angle. Figure 12 demonstrates the insignificant effect caused by two extreme incident angles. As expected, the deviations of the computed results from the measured values increase with flow speeds, which

Table 3 Summary of numerical experiments

	$M_0 = 0$		$M_0 = 0.1$		$M_0 = 0.3$		$M_0 = 0.5$	
f_e, kHz	$\|W'\|$	Agreement	$\|W'\|$	Agreement	$\|W'\|$	Agreement	$\|W'\|$	Agreement
0.5	0.7932	Poor	0.8017	Poor	0.8186	Poor	0.8341	Poor
1.0	0.3704	Good	0.3287	Good	0.2527	Fair	0.1853	Good
1.5	0.5538	Good	0.5744	Fair	0.6131	Poor	0.6471	Fair
2.0	0.6668	Good	0.6925	Fair	0.7335	Fair	0.7648	Fair
2.5	0.5686	Good	0.5914	Fair	0.6322	Poor	0.6670	Fair
3.0	0.2297	Good	0.2010	Good	0.1709	Good	0.1750	Good

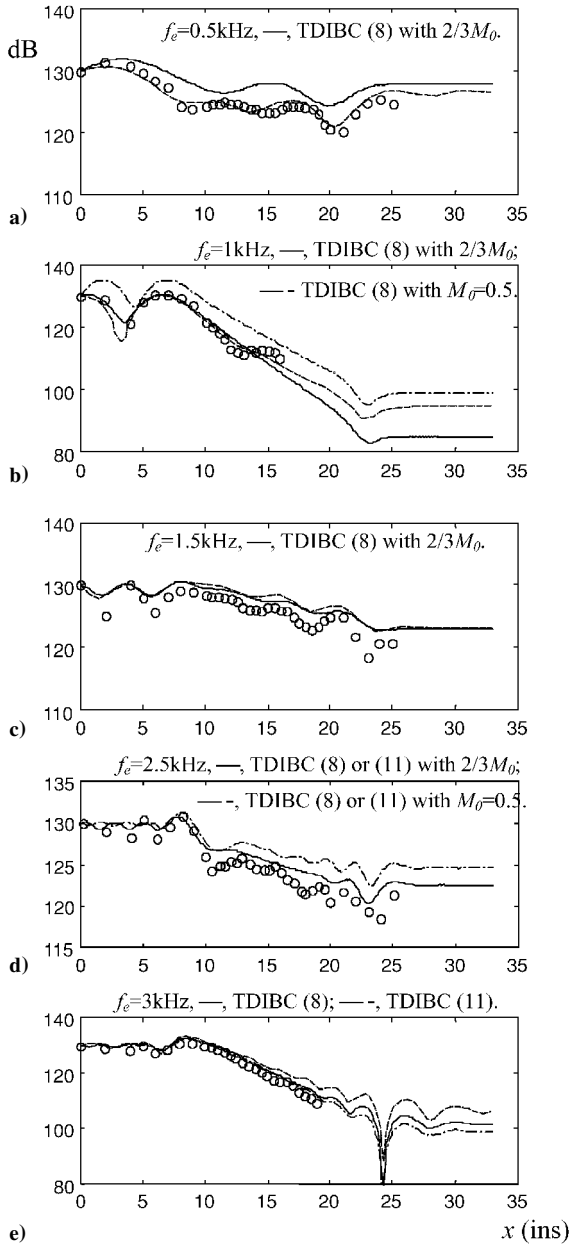

Fig. 8 Sound pressure along the upper wall at different frequencies in slip flow M_0 = 0.5 but using the effective speed $M_{ave} = 2/3M_0$: ∘∘∘, experiment, and - - - -, Ref. 14.

suggests that should effects of the flow profile across the tube be taken into account, the computed results would improve, especially for high wall reflection at the low frequency 0.5 kHz.

Shear Flow Effect

To study the refraction effect caused by a shear flow, we consider the parabolic Mach-number profile across the duct width H for the fully developed laminar channel flow:

$$M_x(y) = 4M_0(y/H)(1 - y/H)$$

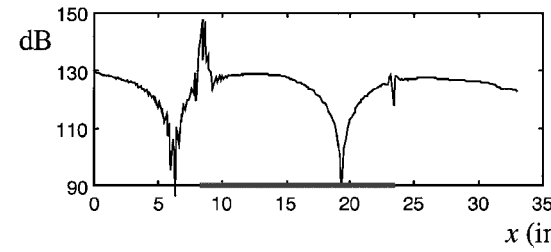

Fig. 9 Sound pressure along the lower wall with impedance material from 8.25 to 23.5 in. using TDIBC (11), slip flow M_0 = 0.3, and f_e = 0.5 kHz.

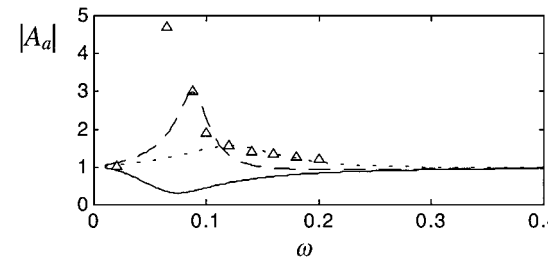

Fig. 10 Variation of $|A_a|$ with ω for slip flow M_0 = 0.3, $Z = 0.41 + i(-0.05416/\omega + 9.75\omega)$: ——, $k_x = \omega/(1 + M_0 \sin\theta)$; - - -, k_x = 0.5; - - - -, k_x = 1; and △, most amplified wave numbers k_x.

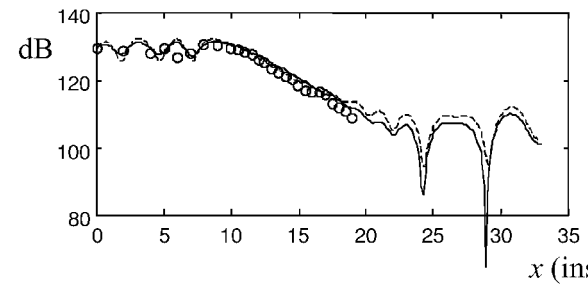

Fig. 11 Sound pressure along the upper wall for slip flow M_0 = 0.5 and f_e = 3 kHz: ——, TDIBC (11) with spatial derivative smoothing; - - - -, TDIBC (8); and ∘∘∘, experiment.

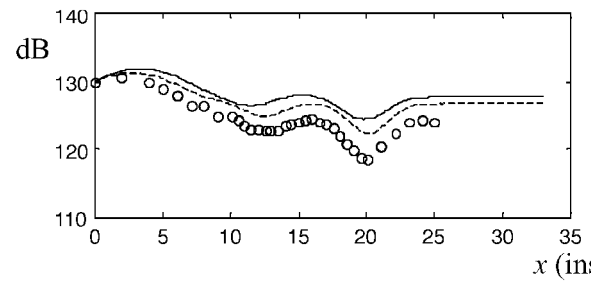

Fig. 12 Sound pressure along the upper wall for f_e = 0.5 kHz and slip flow M_{ave} = 0.333: ——, TDIBC (8) with θ = 90 deg; - - - -, TDIBC (8) θ = 0 deg; and ∘∘∘, experiment.

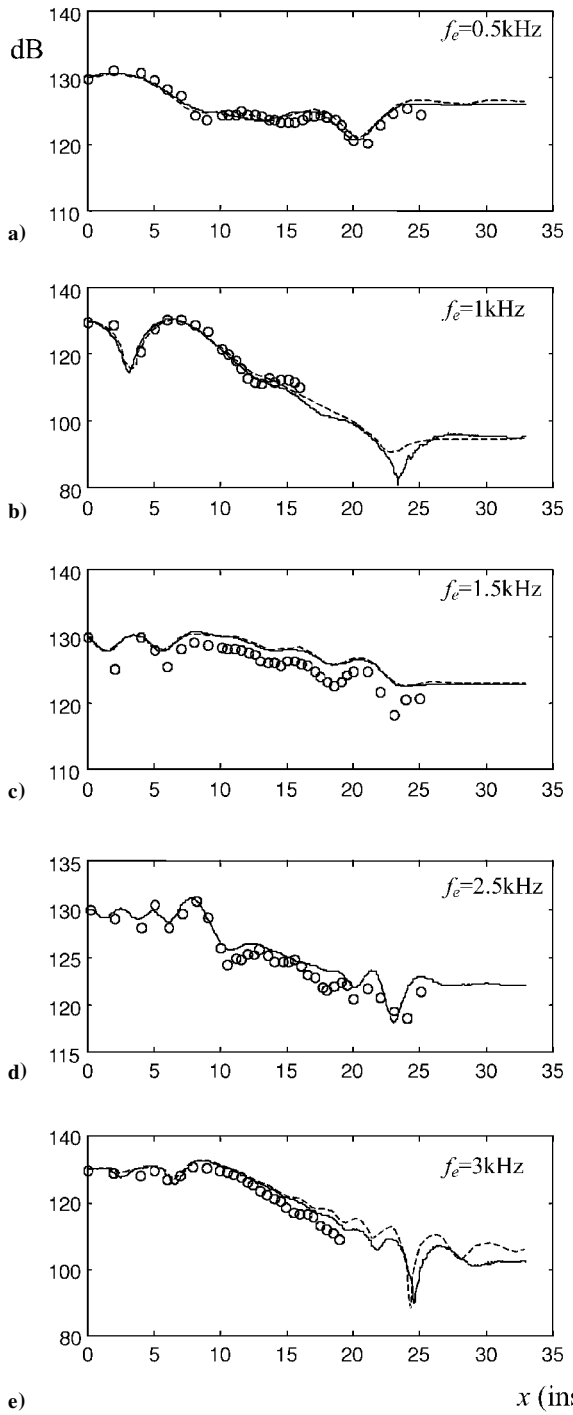

Fig. 13 Sound pressure along the upper wall at different frequencies in shear flow $M_0 = 0.5$: ——, present calculation with sheared velocity; ∘∘∘, experiment; and - - - -, Ref. 14.

Because $M_x(0) = 0$, TDIBC for this case should simply be the same as the classically defined acoustic impedance at zero flow condition. Figure 13a shows the marked improvement of computed results for the highly reflective impedance at 0.5 kHz. The improvement for absorptive walls at other frequencies is not as evident (Figs. 13b and 13e), for which a slip flow with the effective plane-wave impedance Eq. (7) is adequate. The effects of a turbulent boundary layer have also been studied using a $\frac{1}{7}$-power Mach-number profile but to no improvement over the laminar model.

Conclusions

It is shown here that the effective plane-wave impedance provides a simple and satisfactory account of wave refraction in a shear flow for walls with high absorption. Its implementation as TDIBC via the approach of Fung et al.[11] is straightforward and unconditionally stable. The implementation of convection-modified impedance as TDIBC leads to the amplification of numerically supported spurious waves at impedance discontinuity. Although this instability can be suppressed, the convection-modified impedance gives no apparent advantage over the simple effective plane-wave impedance. For highly reflective walls in high-speed flows, refraction effects in a shear layer must be considered. The approach of Fung et al.[17] has been extended here to include effects of a nonuniform flow and TDIBC for efficient aeroacoustics computation.

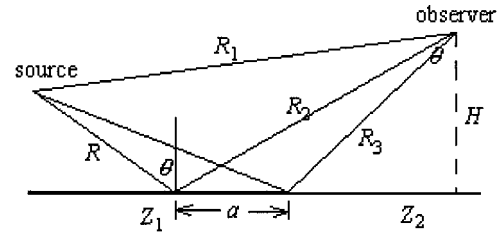

Fig. A1 Point source reflection at a mixed impedance wall.

Appendix: Analytical Plane Wave Reflection at Mixed Impedance Wall

The pressure Fourier component with $\exp(i\omega t)$ caused by a monopole source over a mixed impedance wall can be derived from De Jong's model [Ref. 21, Eq. (4)]:

$$\hat{p} = \begin{cases} \hat{p}_1 + Q_1\hat{p}_2 + (Q_2 - Q_1)\left[\exp(i\pi/4)/\sqrt{\pi}\right](R_1/R_3) \\ \quad \times [F(\chi_{31})\hat{p}_1 + F(\chi_{32})\hat{p}_2], \qquad a \geq 0 \\ \hat{p}_1 + Q_2\hat{p}_2 + (Q_2 - Q_1)[\exp(i\pi/4)/\sqrt{\pi}](R_1/R_3) \\ \quad \times [F(\chi_{31})\hat{p}_1 - F(\chi_{32})\hat{p}_2], \qquad a < 0 \end{cases} \tag{A1}$$

where Q_1, Q_2 are spherical wave reflection coefficients corresponding to impedance Z_1 and Z_2, respectively; a is the distance from the impedance discontinuity to the specula point, R_1 is the direct path length from source to observer (Fig. A1), R_2 the length through the specula point, and R_3 through the impedance discontinuity; $\hat{p}_1 = \exp(-ikR_1)/(kR_1)$ is the direct wave pressure, $\hat{p}_2 = \exp(-ikR_2)/(kR_2)$ the wave through the specula reflection point ($k = \omega$); and $\chi_{31} = \sqrt{[k(R_3 - R_1)]}$, $\chi_{32} = \sqrt{[k(R_3 - R_2)]}$, and the Fresnel integral function

$$F(x) \equiv \int_x^\infty \exp(-it^2)\,dt$$

By taking the limit[22]

$$\bar{\hat{p}} = \lim_{R\to\infty} [\hat{p}/\exp(-ikR)/(kR)]$$

where R denotes the length from source to specula point, Eq. (A1) can be simplified to

$$\bar{\hat{p}} = \begin{cases} \bar{\hat{p}}_1 + \bar{Q}_1\bar{\hat{p}}_2 + (\bar{Q}_2 - \bar{Q}_1)\left[\exp(i\pi/4)/\sqrt{\pi}\right] \\ \quad \times [F(\bar{\chi}_{31})\bar{\hat{p}}_1 + F(\bar{\chi}_{32})\bar{\hat{p}}_2], \qquad a \geq 0 \\ \bar{\hat{p}}_1 + \bar{Q}_2\bar{\hat{p}}_2 + (\bar{Q}_2 - \bar{Q}_1)\left[\exp(i\pi/4)/\sqrt{\pi}\right] \\ \quad \times [F(\bar{\chi}_{31})\bar{\hat{p}}_1 - F(\bar{\chi}_{32})\bar{\hat{p}}_2], \qquad a < 0 \end{cases} \tag{A2}$$

where $\bar{\hat{p}}_1 = \exp[-ik(x\sin\theta - y\cos\theta)]$, $\bar{\hat{p}}_2 = \exp[-ik(x\sin\theta + y\cos\theta)]$, $\bar{Q}_{1,2} = (Z_{1,2}\cos\theta - 1)/(Z_{1,2}\cos\theta + 1)$, $\bar{\chi}_{31} = \sqrt{\{k[a\sin\theta - H(\sin\theta tg\theta - \cos\theta) + H']\}}$, $\bar{\chi}_{32} = \sqrt{[k(a\sin\theta - H/\cos\theta + H')]}$, and $H' = \sqrt{[H^2 + (Htg\theta - a)^2]}$.

Acknowledgments

Financial support on PolyU Grant G-YW23 and computer support on PolyU Grant G-S735 are acknowledged. Thanks are also given to K. M. Li of the Hong Kong Polytechnic University for the helpful discussion on the solution of mixed impedance wall.

References

[1]Hanson, D. B., "Shielding of Prop-Fan Cabin Noise by the Fuselage Boundary Layer," *Journal of Sound and Vibration*, Vol. 92, No. 4, 1984, pp. 591–598.

[2]Campos, L. M. B. C., Serrao, P. G. T. A., Oliveira, J. M. G. S., and Kobayashi, M. H., "On the Acoustics and Stability of Low- and High-Speed Shear Flows," CEAS/AIAA Paper 95-013, 1995.

[3]Brand, R. S., and Nagel, R. T., "Reflection of Sound by a Boundary Layer," *Journal of Sound and Vibration*, Vol. 85, No. 1, 1982, pp. 31–38.

[4]Mu, S., and Mahalingam, S., "Direct Numerical Simulation of Acoustic/Shear Flow Interactions in Two-Dimensional Ducts," *AIAA Journal*, Vol. 34, No. 2, 1996, pp. 237–243.

[5]Cumming, A., and Chang, I.-J., "Acoustic Propagation in Porous Media with Internal Mean Flow," *Journal of Sound and Vibration*, Vol. 114, No. 3, 1987, pp. 565–581.

[6]Wang, M., and Kassoy, D. R., "Transient Acoustic Processes in a Low-Mach-Number Shear Flow," *Journal of Fluid Mechanics*, Vol. 238, 1992, pp. 509–536.

[7]Nayfeh, A. H., Kaiser, J. E., and Telionis, D. P., "Acoustics of Aircraft Engine-Duct Systems," *AIAA Journal*, Vol. 13, No. 2, 1975, pp. 130–153.

[8]Chagelishvili, G. D., Khujadze, G. R., Lominadze, J. G., and Rogava, A. D., "Acoustic Waves in Unbounded Shear Flows," *Physics of Fluids*, Vol. 9, No. 7, 1997, pp. 1955–1962.

[9]Ingard, U., "Influence of Fluid Motion Past a Plane Boundary on Sound Reflection, Absorption, and Transmission," *Journal of the Acoustical Society of America*, Vol. 31, No. 7, 1959, pp. 1035,1036.

[10]Myers, M. K., "On the Acoustic Boundary Condition in the Presence of Flow," *Journal of Sound and Vibration*, Vol. 71, No. 3, 1980, pp. 429–434.

[11]Fung, K.-Y., Ju, H. B., and TallaPragada, B., "Impedance and Its Time-Domain Extensions," *AIAA Journal*, Vol. 38, No. 1, 2000, pp. 30–38.

[12]Tam, C. K. W., and Auriault, L., "Time-Domain Impedance Boundary Conditions for Computational Acoustics," *AIAA Journal*, Vol. 34, No. 5, 1996, pp. 917–923.

[13]Özyörük, Y., Long, L. N., and Jones, M. G., "Time-Domain Numerical Simulation of a Flow-Impedance Tube," *Journal of Computational Physics*, Vol. 146, No. 1, 1998, pp. 29–57.

[14]Özyörük, Y., and Long, L. N, "Time-Domain Calculation of Sound Propagation in Lined Ducts with Sheared Flows," *AIAA Journal*, Vol. 38, No. 5, 2000, pp. 768–773.

[15]Fung, K.-Y., and Ju, H., "Broadband Time-Domain Impedance Models," *AIAA Journal*, Vol. 39, No. 8, 2001, pp. 1449–1454.

[16]Goldstein, M. E., and Rice, E., "Effect of Shear on Duct Wall Impedance," *Journal of Sound and Vibration*, Vol. 30, No. 1, 1973, pp. 79–84.

[17]Fung, K.-Y., Man, R. S., and Davis, S., "An Implicit High-Order Compact Algorithm for Computational Acoustics," *AIAA Journal*, Vol. 34, No. 10, 1996, pp. 2029–2037.

[18]Giles, M. B., "Nonreflecting Boundary Conditions for Euler Equation Calculations," *AIAA Journal*, Vol. 28, No. 12, 1990, pp. 2050–2058.

[19]Morse, P. M., and Ingard, K. U., *Theoretical Acoustics*, McGraw–Hill, New York, 1968.

[20]Parrott, T. L., Watson, W. R., and Jones, M. G., "Experimental Validation of a Two-Dimensional Shear Flow Model for Determining Acoustic Impedance," NASA TP-2679, 1987.

[21]Boulanger, R., Waters-Fuller, T., Attenborough, K., and Li, K. M., "Models and Measurements of Sound Propagation from a Point Source over Mixed Impedance Ground," *Journal of the Acoustical Society of America*, Vol. 102, No. 3, 1997, pp. 1432–1442.

[22]Naghieh, M., and Hayek, S. I., "Diffraction of a Point Source by Two Impedance Covered Half-Planes," *Journal of the Acoustical Society of America*, Vol. 69, No. 3, 1981, pp. 629–637.

P. J. Morris
Associate Editor